Pattern Detection in Images using LBP-based Relational Operators

José M. Molina-Casado and Enrique J. Carmona

Dpto. de Inteligencia Artificial, ETSI Informática, Universidad Nacional de Educación a Distancia (UNED), Juan del Rosal 16, 28040, Madrid, Spain
jmolina_79@hotmail.com
ecarmona@dia.uned.es

Abstract. This paper describes two new pattern detection image operators, $\Re_1^{riu2}$ and $\Re_2$, called, in a generic way, LBP-based relational operators (LBP-RO). The former is rotational invariant and allows searching for a particular pattern disposes in any direction, the later is a binary operator designed to find image patterns that can be modeled by a pattern function. Both of them are invariants against any monotonic transformation of the image gray scale. We have applied these operators in a case study dedicated to segment the ONH in eye fundus color photographic images. The new segmentation method, called GA+LBP-RO, was compared to a competitive ONH segmentation method in the literature and the results obtained by our method proved to be equal to or better.

Keywords: Local Binary Pattern (LBP), Relational Operator, Genetic Algorithm, ONH Segmentation.

1 Introduction

Local Binary Patterns (LBP) are a type of features used for classification in computer vision [6]. The calculation of that feature consists in comparing the intensity of a pixel, g_c, with its neighboring pixels, g_p, and considering the result of each comparison as a bit in a binary string. In that comparison, only the sign, $s(x)$, is considered:

$$s(x) = \begin{cases} 1, & x \geq 0 \\ 0, & x < 0 \end{cases} \tag{1}$$

By assigning a binomial factor 2^p for each comparison, $s(g_p - g_c)$, we obtain a unique $LBP_{P,R}$ number that characterizes the spatial structure of the local image texture:

$$LBP_{P,R} = \sum_{p=0}^{P-1} s\left(g_p - g_c\right) 2^p \tag{2}$$

where P controls the number of neighboring pixels, and R determines the radial distance of the these pixels to the central pixel. As a advantage, $LBP_{P,R}$ operator is by definition invariant against any monotonic transformation of the image gray scale.

A extension to the LBP original operator is $LBP^{riu2}_{P,R}$, described in [7]:

$$LBP^{riu2}_{P,R} = \begin{cases} \sum_{p=0}^{P-1} s\left(g_p - g_c\right) & if\ U\left(LBP_{P,R}\right) \leq 2 \\ P+1 & otherwise \end{cases} \tag{3}$$

where the superscript $riu2$ reflects the use of rotation invariant uniform patterns that have U value of at most 2, and $U(.)$ is a uniformity measure defined by:

$$U(LBP_{P,R}) = \left|s\left(g_0 - g_c\right) - s\left(g_{P-1} - g_c\right)\right| + \sum_{p=1}^{P-1} \left|s\left(g_p - g_c\right) - s\left(g_{p-1} - g_c\right)\right| \tag{4}$$

Thus, if $U(LBP_{P,R}) \leq 2$, then $LBP^{riu2}_{P,R}$ is calculated by counting the number of ones in the binary string $LBP_{P,R}$; otherwise all the other patterns are labeled as "miscellaneous" and collapsed into one value $P+1$. This operator is an excellent measure of the spatial structure of local image texture and is invariant to rotations and against any monotonic transformation of the gray scale.

The idea of the LBP operator can be also extended by using relational functions [8]:

$$\Re\left(x, y, r_1, r_2, \phi, n\right) \rightarrow [0,1]^n \tag{5}$$

This function is calculated on a point (x, y) of the image, comparing the intensity of n equidistant pairs of points located, respectively, to a distance r_1 and r_2 from the point (x, y). The radial vectors, r_1 and r_2, always form a constant angle defined by ϕ. Based on different combinations of r_1,r_2 and ϕ, local information at different scales and orientations can be captured. However, that function does not provide rotational invariance.

Taking the above defined operators as inspiration, we describe in this paper two new operators, denoted by $\Re^{riu2}_1$ and $\Re_2$. The former is a rotational invariant extension of $\Re$ and the later is a LBP-based binary operator designed to find image patterns that can be modeled by a function.

The article is organized as follows. Section 2 describes the two new operators mentioned. In section 3, we test the performance of such operators to detect patterns in a case study: segmentation of the optic nerve head in eye fundus images. Finally, section 4 presents the conclusions and future work.

2 LBP-based Relational Operators

In this section, we describe two new image operators, $\Re^{riu2}_1$ and $\Re_2$, based on the concepts of LBP [6, 7] and relational function [8]. They will be called, in a

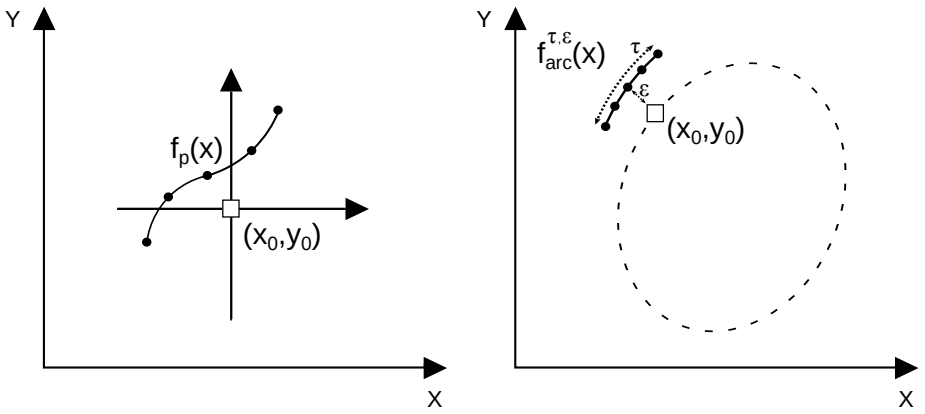

(a) (b)

Fig. 1: Examples of pattern functions, $f_p(x)$, defined in a image point (x_0, y_0): (a) generic function (b) ellipse arc function, $f_{arc}^{\tau,\varepsilon}(x)$.

generic way, LBP-based relational operators (LBP-RO). On the one hand, $\Re_1^{riu2}$ corresponds to an extension of (5) and is defined by:

$$\Re_1^{riu2}(x, y, r_1, r_2, \phi, n) \rightarrow \{0, 1, ..., (n+1)\} \tag{6}$$

Here, the idea is to add rotational invariance, using the concept of uniformity measure defined in (4). Thus, the computation of this operator is given by:

$$\Re_1^{riu2}(x, y, r_1, r_2, \phi, n) = \begin{cases} \sum_{k=0}^{n-1} R_{1k} & if\, U(R_{1k}) \leq 2 \\ n+1 & otherwise \end{cases} \tag{7}$$

where

$$R_{1k} = s(g(x_2, y_2) - g(x_1, y_1)), \quad k = 0, 1, \ldots, (n-1) \tag{8}$$

$$U(R_{1k}) = \mid R_{10} - R_{1(n-1)} \mid + \sum_{k=1}^{n-1} \mid R_{1k} - R_{1(k-1)} \mid \tag{9}$$

and the coordinates of each pair of points to compare is given by

$$(x_1, y_1) = (x + r_1 \cdot cos(k \cdot 2\pi/n), y + r_1 \cdot sin(k \cdot 2\pi/n) \tag{10}$$

$$(x_2, y_2) = (x + r_2 \cdot cos(k \cdot 2\pi/n + \phi), y + r_2 \cdot sin(k \cdot 2\pi/n + \phi) \tag{11}$$

On the other hand, the second relational operator, $\Re_2$, is defined by

$$\Re_2\,(x, y, \mathcal{H}_{x_i,y_i}, f_p(x), n) \rightarrow \{0, 1\} \tag{12}$$

where (x, y) are the coordinates of the image pixel on which the operator is applied, and $\mathcal{H}_{x_i,y_i} = \{(x_i, y_i) \,|\, y_i = f_p(x_i),\ i = 1, ..., n\}$ is a set of n points resulting from sampling the $f_p(x)$ function, called *pattern function* (see figure 1a). The computation of this operator consists in comparing the intensity value of the pixels belonging to $\mathcal{H}_{x_i,y_i}$ with the intensity value of the reference pixel, according to the following criteria:

$$\Re_2(x, y, \mathcal{H}_{x_i,y_i}, f_p(x), n) = \begin{cases} 1 & if\ g(x_i, y_i) \geq g(x, y), \forall i \epsilon \{1, \ldots, n\} \\ 0 & otherwise \end{cases} \tag{13}$$

Note that the purpose of this relational operator is to identify a particular pattern, defined by $f_p(x)$, in the neighborhood of the analysis point.

3 Case Study: Segmenting the ONH

The segmentation of the optic nerve head (ONH) is of critical importance in retinal image analysis because ONH disturbances can be an initial symptom of serious eye diseases. The ONH, also called optic disk or papilla, is oval-shaped and is located in the area where all the retina nerve fibres come together to form the start of the optic nerve that leaves the back of the eyeball. There is an area without any nerve fibres called excavation (the centre of the papilla) and around it another area can be found, the neuroretinal ring, whose external perimeter delimits the papillary contour.

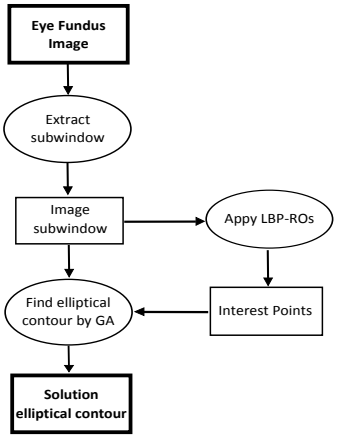

Fig. 2: Block diagram summarizing the proposed method to segment the ONH.

The segmentation method here used is a variation of the method described in [3] and with which will be compared (see Section 3.2). The main difference

between both methods lies in how to get the set of interest points (IPs). Here, the IPs are obtained using LBP-ROs and, in the original method, they are obtained using a domain-knowledge-based *ad-hoc* method. First of all, in order to reduce the processing computational cost and the number of distractor patterns, the process begins by automatically extracting a sub-window from the original image that is approximately centered at a point of the papillary area [5]. Next, the two LBP-ROs above defined are applied to the image sub-window[1] and the result is a set of IPs points that have a high probability of belonging to the papillary contour. Then, we use a genetic algorithm (GA) to find an ellipse whose contour is formed by the maximum number of interest points. Finally, we select the best genetic ellipse (papillary contour) from the final population as the solution to our problem. The figure 2 summarizes the process.

3.1 LBP-RO Instantiation

Taking advantage of the characteristics of the operator $\Re_2$, we proceed as follows. Given an generic ellipse traced in the retinal image, $\Re_2$ is applied only and exclusively to those pixels belonging to the contour of this ellipse. To do that, a function denoted by $f_{arc}^{\tau,\varepsilon}(x)$ is defined for each pixel of the contour. That function corresponds to an ellipse arc which is parallel to the considered ellipse, has a length, τ, and is separated a distance, ε, (towards its outer side) from the analysis pixel (x, y) (see figure 1b). This operator, thus instantiated, will be hereinafter denoted by $\Re_{2\_0}$:

$$\Re_{2\_0} = \Re_2(x, y, \mathcal{H}_{x_i,y_i}, f_{arc}^{\tau,\varepsilon}(x), n) \tag{14}$$

The better the ellipse approximates the contour papillary, the greater the number of pixels belonging to the ellipse contour that satisfy$\Re_{2_0} = 1$. This follows from the definition of this operator and the property of the papillary contour: frontier that separates the papilla (bright area) from the retina (darker area). However, since infinite ellipses can be traced in the image, we will use a genetic algorithm in order to search the optimal ellipse. To code this type of solutions, the phenotypic space is transformed into a genotypic space consisting of real vectors of five variables $[x, y, a, b, \theta]$, where (x, y) represents the centre of the genetic ellipse, (a, b) the magnitudes of its major and minor semi-axis respectively and θ the angle that its major axis forms with the x-axis. Finally, by applying recombination, mutation and selection operators, a population of chromosomes (ellipses) evolves until a finalization criterion is achieved. The degree of approximation to the solution of each ellipse can be calculated using the following fitness function:

$$f_{fitness_1} = \sum_{(x_k,y_k)\in GEC} \Re_{2\_0}(x_k, y_k, \mathcal{H}_{x_i,y_i}, f_{arc}^{\tau,\varepsilon}(x), n) \tag{15}$$

[1] Specifically, the operators are applied to the V channel as result of transforming the original RGB color space into HSV space.

where GEC is the genetic ellipse contour. That is, this operator computes the number of pixels belonging to GEC that satisfy $\Re_{2\_0} = 1$.

However, it is possible to refine the fitness function defined in (15). One must take into account that the vessels are also delimited by boundaries separating the retina (brighter areas) from the vessels (darker areas). So if we only applied the fitness function defined in (15), the papillary contour could be formed by a genetic ellipse whose contour pixels belong to vessel-retina boundaries or the papillary contour. In order to reduce this possibility, we will use the $\Re_1^{riu2}$ operator, instantiated by $\Re_{1\_0}^{riu2}$:

$$\Re_{1\_0}^{riu2} = \Re_1^{riu2}(x, y, r, r, \pi, 8) \tag{16}$$

where r is a value bigger than the width of any vessel in the image. Here we use the geometric property by which the width of a vessel is always smaller than the width of the papilla. Then it is not difficult to check that, if a pixel belongs to the papillary contour, we will obtain, with high probability, a value belonging to the set $\{4, 5\}$, as result of applying $\Re_{1\_0}^{riu2}$ to that pixel. Note that these two values correspond, respectively, to patterns 00001111 (or their equivalents rotated) and 00011111 (or their equivalents rotated). On the other hand, if the same operator is applied to a pixel belonging to the contour of a vessel, assuming uniform retinal intensities and linear vessel shapes in the zone in which the operator acts, we will obtain, with high probability, a value belonging to the set $\{7, 8\}$. Note that these two values correspond respectively to patterns 01111111 (or their equivalents rotated) and 11111111. The interesting thing about these two pattern sets is that they are disjoint. However, in real situations, there is noise in the image, that is, the retina is not always uniform, there are papillary contour zones that are traversed by vessels and these vessels can be formed by curved paths or branches. Therefore, the final idea is to use the two operators, $\Re_{1\_0}^{riu2}$ and $\Re_{2\_0}$, together to promote the synergy of detecting only papillary contour points and avoid the occurrence of false positives. From the point of view of the GA, it only involves changing the fitness function defined in (15) by this other:

$$f_{fitness_2} = \sum_{i=1}^{n} and\left(\Re_{1\_\{4,5\}}^{riu2}, \Re_{2\_0}\right) \tag{17}$$

where

$$\Re_{1\_\{4,5\}}^{riu2} = \begin{cases} 1 & if\ (\Re_{1\_0}^{riu2}) \in \{4, 5\} \\ 0 & otherwise \end{cases} \tag{18}$$

Finally, figure 3 shows two examples of how work the two LBP-OP in two different genetic ellipses (upper row and lower row). The figures 3a and 3b are the result of applying the operators $\Re_{2\_0}$ and $\Re_{1\_\{4,5\}}^{riu2}$, respectively, to the same genetic ellipse, and figure 3c shows the result of applying the *and* operator. Similar comments apply to lower row figures. It is easy to check that the total number of points that verify both criteria ($\Re_{2\_0} = 1$ and $\Re_{1\_\{4,5\}}^{riu2} = 1$) is greater

for the upper row ellipse (figure 3c) than the lower row one (figure 3f). Therefore, the former will be a better approach to the papillary contour than the later one.

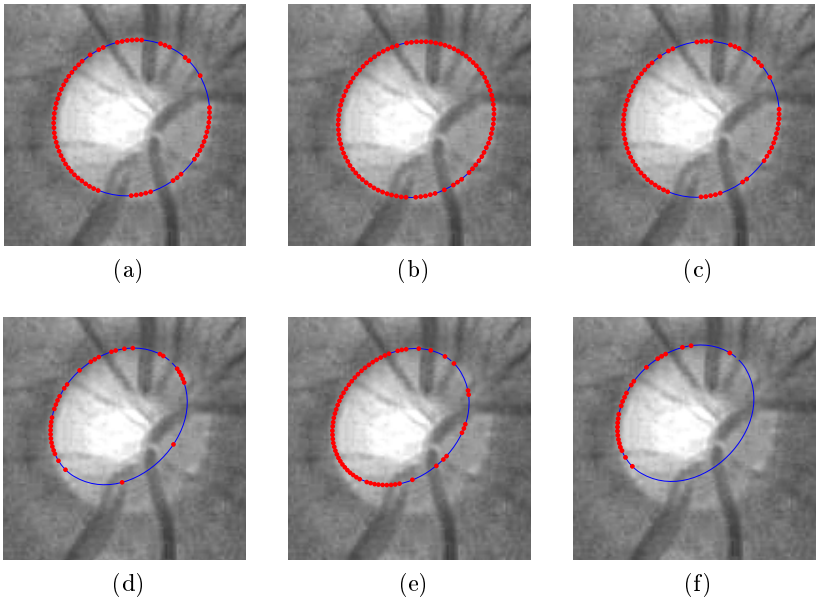

Fig. 3: Example of applying LBP-ROs to two different genetic ellipses (upper row and lower row): (a)&(d) $\Re_{2\_0}$; (b)&(e) $\Re^{riu2}_{1\_\{4,5\}}$; (c)&(f) *and* $\left(\Re_{2\_0}, \Re^{riu2}_{1\_\{4,5\}}\right)$.

3.2 Results and Evaluation

To measure the performance of our algorithm, denoted by GA+LBP-RO, we used DRIONS [1, 3] and ONHSD [2, 4] databases. In order to do the segmentation results quantitatively reproducible, we measured the average discrepancy between the points of the contour obtained with the segmentation method and a gold standard defined from a contour that was the result of averaging several contours, each of them traced by an expert (two experts in DRIONS and four in ONHSD). Here we use the concept of discrepancy, δ, defined in [4]:

$$\delta^j = \frac{\sum_{i=1}^{N}((\mid m_i^j - \mu_i^j \mid)/(\sigma_i^j + \varepsilon))}{N} \tag{19}$$

where δ^j is the discrepancy measurement for the image j, $i = 1, ..., N$, with N the number of angularly equidistant radial segments used for each measurement, m_i^j is the length of the radius defining the i-th point of the ellipse proposed for the image j, μ_i^j and σ_i^j are the mean and typical deviation, respectively, of the

lengths of the radii defining the i-th point of the contours traced by the experts and belonging to the image j, and $\varepsilon = 0.5$ is a small factor to prevent division by zero when the experts are in exact agreement. To facilitate the visualization of the results, a discrepancy curve is plotted, namely, the percentage of images with discrepancy less than δ (y-axis) versus δ (x-axis).

The parameter configuration used for the GA was the same as that used in [3]. For the operator $\Re^{riu2}_{1\_\{4,5\}}$, the following final parameter configuration was chosen: $\Re^{riu2}_{1\_\{4,5\}}(x, y, 10, 10, \pi, 8)$ for DRIONS and $\Re^{riu2}_{1\_\{4,5\}}(x, y, 8, 8, \pi, 8)$ for ONHSD. For the $\Re_{2\_0}$ operator and for both databases, the final parameter configuration was $\Re_{2\_0}(x, y, \mathcal{H}_{x'_i, y'_i}, f^{8,2}_{arc}(x), 8)$.

The results obtained were compared with the segmentation method described in [3]. Thus, the figure 4 shows the discrepancy curves obtained from applying the two methods to each image database. Owing to the stochastic nature associated with the GA, each curve of discrepancy showed (both methods use a GA-based approach) correspond to the result of averaging five curves obtained as a result of executing the GA five times.

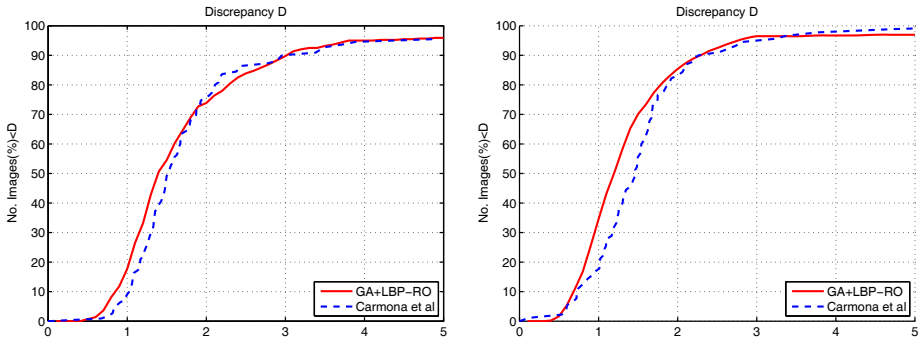

Fig. 4: Accumulated discrepancy results for our method, GA+LBP-RO, versus the segmentation method described in [3]: (a) DRIONS and (b) ONHSD databases.

Looking at the figure 4, we can say that practically our method improves or equals the performances of the other method in both databases. Beside, it must be said that the procedure used by GA+LBP-RO to obtain the interest points is more simple than that one used in [3]. Finally, we must emphasize that, unlike the method with which is compared, GA+LBP-RO does not use any kind of normalization in the images database[2]. That is possible because the two LBP-RO used are invariant against any monotonic transformation of the images gray

[2] In figure 4, the discrepancy curves of GA+LBP-RO were obtained without normalizing the databases.

scale. We have made experiments applying and not applying this normalization phase (see figure 5). It is easy to see that, in both databases, the normalization phase does not contribute to improve the discrepancy curves.

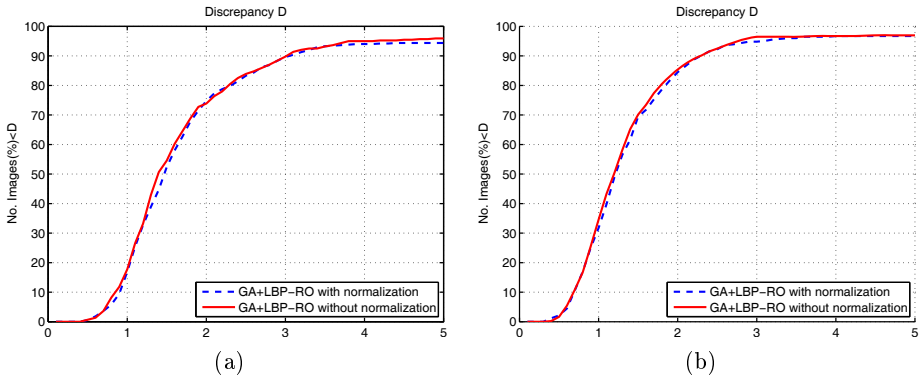

Fig. 5: Discrepancy curves, using GA+LBP-RO, with and without normalizing the image databases: (a) DRIONS (b) ONHSD.

4 Conclusions and Future Work

We have described two new image operators, $\Re_1^{riu2}$ and $\Re_2$, called LBP-based relational operators. The former is rotational invariant and allows searching for a particular pattern disposes in any direction and computed from a symmetric neighborhood. The later is not rotational invariant but allows searching for patterns modeled by an asymmetric neighborhood characterized by a pattern function, $f_p(x)$. Both of them are invariant against any monotonic transformation of the gray scale. We have applied these operator successfully in a segmentation method, called GA+LBP-RO, used to segment the ONH in eye fundus color photographic images. The performances of GA+LBP-RO were compared to a competitive method in the literature and the results obtained by our method proved to be equal to or better. As future work, we propose to investigate other types of LBP-RO and apply them to other image databases and other domains.

Acknowledgment

This work was supported in part by funds of the Advanced Artificial Intelligence Master Program of the Universidad Nacional de Educación a Distancia (UNED), Madrid, Spain.

References

1. DRIONS-DB: Digital retinal images for optic nerve segmentation database. http://www.ia.uned.es/personal/ejcarmona/DRIONS-DB.html, January 2013.
2. ONHSD: Optic nerve head segmentation dataset. http://reviewdb.lincoln.ac.uk/Image%20Datasets/ONHSD.aspx, January 2013.
3. E.J. Carmona, M. Rincón, J. García-Feijoo, and J. M. Martínez-de-la Casa. Identification of the optic nerve head with genetic algorithms. *Artificial Intelligence in Medicine*, 43:243–259, 2008.
4. J. Lowell, A. Hunter, D. Steel, A. Basu, R. Ryder, and E. Fletcher. Optic nerve head segmentation. *IEEE Transaction on Medical Imaging*, 23(2):256–264, 2004.
5. J.M. Molina and E.J. Carmona. Localization and segmentation of the optic nerve head in eye fundus images using pyramid representation and genetic algorithms. In J.M. Ferrández et al, editor, *Foundations on Natural and Artificial Computation*, volume LNCS-6686, pages 431–440. Springer-Verlag, 2011.
6. T. Ojala, M. Pietikäinen, and D. Harwood. A comparative study of texture measures with classification based on featured distributions. *Pattern Recognition*, 29:51–59, 1996.
7. T. Ojala, M. Pietikäinen, and T. Mäenpää. Multiresolution gray-scale and rotation invariant texture classification with local binary patterns. *IEEE Transactions on Pattern Analysis and Machine Intelligence*, 24:971–987, 2002.
8. L. Setia, A. Teynor, A. Halawani, and H. Burkhardt. Grayscale medical image annotation using local relational features. *Pattern Recognition Letters*, 29:2039–2045, 2008.